View metadata, citation and similar papers at core.ac.uk
brought to you by CORE
provided by Ghent University Academic Bibliography

25th International Congress on Sound and Vibration
8-12 July 2018 HIROSHIMA CALLING
ICSV25

QUANTIFYING PERFORMANCE OF MULTI-MODAL TARGETED ENERGY TRANSFER OF A BI-STABLE NONLINEAR PASSIVE VIBRATION ABSORBER

Kevin Dekemele, Robin De Keyser, Mia Loccufier
Ghent University, Departement of Electrical Energy, Metals, Mechanical Construction and Systems , 9052 Ghent, Belgium, email: kevin.dekemele@ugent.be

To passively reduce vibrations in mechanical systems, a linear mass spring damper system, called a tuned mass damper (TMD), is locally added. A TMD is only capable of mitigating vibrations at a single frequency. If this frequency shifts, the linear TMD will fail to reduce vibrations significantly. TMDs with a nonlinear connecting stiffness, so-called nonlinear energy sinks (NES), absorb vibrations through targeted energy transfer (TET). Not only is the performance more robust w.r.t detuning, a single NES is capable of reducing vibrations of several frequencies through resonance capture cascade (RCC). Typically, performance of a NES is investigated by means of many numeric simulations for different parameters of the coupled system. Here, algebraic performance measures are derived, which quantifies TET and RCC performance without simulations. These measures will investigate the efficiency of a NES having a bistable stiffness, which numerical simulations in literature have hinted to have an increased performance over a monostable NES.

Keywords: passive vibration control, nonlinear energy sink, targeted energy transfer, bi-stable stiffness

1. Introduction

For free vibrating linear lumped MDOF mechanical systems, a single nonlinear energy sink (NES) has the ability to act as a robust TMD both for single and multi-modal vibrations [1]. If these vibrations are single frequency, the mechanism behind this vibration mitigating is called targeted energy transfer (TET). For multi-modal vibrations, a NES can engage in so-called resonance capture cascade (RCC), where the NES mitigates the modal vibrations of the mechanical system sequentially, from high to low frequency. This is in sharp contrast with a linear TMD, which is only capable of absorbing a single frequency. In order to have a well-tuned NES, its performance should be assessed. As the mechanical system and NES yield nonlinear dynamic equations, typically numerical examples are simulated, and performance measures are derived from the result. This is time consuming if the NES performances needs to be investigated for many different parameters. The performance of a NES was defined algebraically in [4] for a monostable NES of qubic power. For given coefficients of the mechanical system and NES, the following performance can be assessed, without any numerical dynamic simulations; the energy dissipated during TET and the pumping time. The energy dissipated during TET expression the fraction of initial energy dissipated during TET, while a residual amount of vibration energy is damped very slowly. The pumping time is how long targeted energy transfer persists for a single modal frequency. Here, a cascading time is defined, the time how long the NES takes to mitigate all the modes partaking in RCC. These measures were derived

by simplifying the nonlinear dynamics with semi-analytic techniques, yielding so-called approximate slow flow dynamics. In [2], numerical simulations show an increased performance of a bi-stable NES w.r.t. a monostable NES. Here, the framework of the algebraic performance measures is expanded to bistable NESs, by having a connecting stiffness with a cubic nonlinearity and a negative linear part. The system possess 3 equilibria, 1 unstable and 2 stable. The performance for vibrations around all equilibria will be investigated. Practically, the NES will always initially be in its stable equilibrium. First, the slow flow dynamics are derived in section 2 and 3, followed by the tuning procedure and definition of the algebraic performance measures in section 4. Finally, the measures are compared to numerical simulations, both for single and multi-modal vibrating system.

2. System dynamics

The considered mechanical system is a linear lumped MDOF with physical coordinate vector $x \in \mathbb{R}^n$. A NES is connected to coordinate x_ℓ. Modal decoupling to modal coordinates $q \in \mathbb{R}^n$ results in n eigenfrequencies ω_i and the eigenvector matrix, $E = [e_1 \quad e_2 \quad \dots \quad e_n] \in \mathbb{R}^{n\times n}$. The modal dynamics are

$$\begin{cases} M_q\ddot{q} + C_q\dot{q} + K_q q + m_{na}e_*(\ell)^T\ddot{x}_{na} = E^T F \\ m_{na}\ddot{x}_{na} + c_{na}(\dot{x}_{na} - \dot{x}_\ell) + k_{na}(x_{na} - x_\ell)^3 - k_{lin}(x_{na} - x_\ell) = 0 \end{cases} \tag{1}$$

with $e_*(\ell) \in \mathbb{R}^{n\times 1}$ the ℓ-th row of E, M_q the modal mass, C_q the modal damping and K_q the modal stiffness matrix. The bistable behavior is introduced by the negative linear part ($-k_{lin}$, with $k_{lin} \in \mathbb{R}^+$). To simplify the analysis, it is assumed that the system vibrates with a single vibration mode i : $x(t) = \sum_{k=1}^n e_k q_k(t) = e_i q_i(t)$. The physical coordinate $x_\ell = e_i(\ell)q_i$ is reintroduced:

$$\begin{cases} \ddot{x}_\ell + \epsilon\lambda\dot{x}_\ell + \omega_i^2 x_\ell + \epsilon\ddot{x}_{na} = 0 \\ \epsilon\ddot{x}_{na} + \epsilon\lambda_{na}(\dot{x}_{na} - \dot{x}_\ell) + \epsilon\Omega\omega_i^4(x_{na} - x_\ell)^3 - \epsilon\kappa\omega_i^2(x_{na} - x_\ell) = 0 \end{cases} \tag{2}$$

with

$$\epsilon\lambda = \frac{c_{q,i}}{m_{q,i}} \quad \omega_i^2 = \frac{k_{q,i}}{m_{q,i}} \quad \epsilon = \frac{m_{na}e_i^2(\ell)}{m_{q,i}} \quad \kappa = \frac{k_{lin}}{m_{na}\omega_i^2} \quad \lambda_{na} = \frac{c_{na}}{m_{na}} \quad \Omega = \frac{k_{na}}{m_{na}\omega_i^4}$$

The $n+1$ DOF problem is reduced to a 2DOF problem because of the single mode assumption. Due to the bi-stable behavior, the system has 3 equilibrium points. The first one, $x^{*,1} = \{x^*_{\ell,1}; x^*_{na,1}\} = \{0, 0\}$, is unstable, while the other two $x^{*2,3} = \left\{x_\ell^{*,2,3}; x_{na}^{*,2,3}\right\} = \left\{0, \pm\frac{1}{\omega_i}\sqrt{\frac{\kappa}{\Omega}}\right\}$ are stable, shown through linearization. The vibrations around the two stable fixed points will be investigated, $\Delta x_\ell = x_\ell$ and $\Delta x_{na} = x_{na} \mp \frac{1}{\omega_i}\sqrt{\frac{\kappa}{\Omega}}$:

$$\begin{cases} \Delta\ddot{x}_\ell + \epsilon\lambda\Delta\dot{x}_\ell + \omega_i^2\Delta x_\ell + \epsilon\Delta\ddot{x}_{na} = 0 \\ \epsilon\Delta\ddot{x}_{na} + \epsilon\lambda_{na}(\Delta\dot{x}_{na} - \Delta\dot{x}_\ell) + \epsilon\Omega\omega_i^4\left(\Delta x_{na} - \Delta x_\ell \pm \dfrac{1}{\omega_i}\sqrt{\dfrac{\kappa}{\Omega}}\right)^3 - \epsilon\kappa\omega_i^2\left(\Delta x_{na} - \Delta x_\ell \pm \dfrac{1}{\omega_i}\sqrt{\dfrac{\kappa}{\Omega}}\right) = 0 \end{cases} \tag{3}$$

The differential equation in (3) does not allow an exact analytic solution. Therefor, semi-analytic techniques are used in the next section yielding an approximate solution.

3. Semi-analytic reduction

A change of variables is performed, $u = \Delta x_l + \epsilon\Delta x_{na}$, the center of mass of modal/absorber system (3), and $v = \Delta x_l - \Delta x_{na}$, the relative absorber movement. (3) is rewritten in the new

coordinates where the terms beyond $\mathcal{O}(\epsilon^2)$ are omitted and $\epsilon\ddot{u} = -\epsilon\omega_i^2 u + \mathcal{O}(\epsilon^2)$.

$$\begin{cases} \ddot{u} + \omega_i^2 u + \epsilon\Big(\lambda\dot{u} + \omega_i^2(v-u)\Big) + \mathcal{O}(\epsilon^2) = 0 \\ \epsilon(\ddot{v} + \omega_i^2 v) + \epsilon\omega_i^2(u-v) + \epsilon\lambda_{na}\dot{v} + \epsilon\Omega\omega_i^4\left(v \pm \frac{1}{\omega_i}\sqrt{\frac{\kappa}{\Omega}}\right)^3 - \epsilon\kappa\omega_i^2\left(v \pm \frac{1}{\omega_i}\sqrt{\frac{\kappa}{\Omega}}\right) + \mathcal{O}(\epsilon^2) = 0 \end{cases} \tag{4}$$

The followed steps are taken to simplify the dynamics; 1) the variables u and v are complexified as $\varphi(t)e^{i\omega_i t} = \dot{u} + i\omega_i u$ and $\varphi_{na}(t)e^{i\omega_i t} = \dot{v} + i\omega_i v$, 2) regular perturbation theory is applied, expanding both complexified variables in a major $\mathcal{O}(\epsilon^0)$ and minor contribution $\mathcal{O}(\epsilon)$: $\varphi = \varphi_0 + \epsilon\varphi_1$ and $\varphi_{na} = \varphi_{na0} + \epsilon\varphi_{na1}$, 3) the dynamics are analyzed as if they depend on two separate time scales, a fast $T_0 = t$ and slow $T_1 = \epsilon t$ time scale, $u(t) = u(T_0, T_1)$, $v(t) = v(T_0, T_1)$. This way, d/dt is a total derivate,$\frac{d}{dt} = \frac{\partial}{\partial T_0} + \epsilon\frac{\partial}{\partial T_1}$. These three operations on (4) result in:

$$\begin{cases} \dfrac{\partial\varphi_0}{\partial T_0} + \epsilon\dfrac{\partial\varphi_0}{\partial T_1} + \epsilon\dfrac{\partial\varphi_1}{\partial T_0} + \epsilon\lambda\dfrac{\varphi_0}{2} + \epsilon\dfrac{\omega_i^2}{2i\omega_i}\big(\varphi_{na0} - \varphi_0\big) + \Big(\epsilon\lambda\dfrac{\bar{\varphi}_0}{2} - \epsilon\dfrac{\omega_i^2}{2i\omega_i}\big(\bar{\varphi}_{na0} - \bar{\varphi}_0\big)\Big)e^{-2i\omega_i t} = 0 \\ \epsilon\left(\dfrac{\partial\varphi_{na0}}{\partial T_0}\right) + \epsilon\dfrac{\omega_i^2}{2i\omega_i}\big(\varphi_0 - \varphi_{na0}\big) + \epsilon\lambda_{na}\dfrac{\varphi_{na0}}{2} - \dfrac{\epsilon\kappa\omega_i^2}{2i\omega_i}\varphi_{na0} \\ \quad + \Big(-\epsilon\dfrac{\omega_i^2}{2i\omega_i}\big(\bar{\varphi}_0 - \bar{\varphi}_{na0}\big) + \epsilon\lambda_{na}\dfrac{\bar{\varphi}_{na0}}{2} + \dfrac{\epsilon\kappa\omega_i^2}{2i\omega_i}\bar{\varphi}_{na0}\Big)e^{-2i\omega_i t} \mp \dfrac{\epsilon\kappa\omega_i^2}{\omega_i}\sqrt{\dfrac{\kappa}{\Omega}}e^{-i\omega_i t} \\ \quad + \epsilon\omega_i^4\Omega \displaystyle\sum_{k_1+k_2+k_3=3}\binom{3}{k_1, k_2, k_3}\dfrac{\varphi_{na}^{k_1}\bar{\varphi}_{na}^{k_2}}{(2i\omega_i)^{k_1+k_2}}\left(\pm\dfrac{1}{\omega_i}\sqrt{\dfrac{\kappa}{\Omega}}\right)^{k_3} e^{i(k_1-k_2-1)\omega_i t} = 0 \end{cases} \tag{5}$$

with the bar sign denoting a complex conjugate and the last term being the multinomial expansion for power 3. To ensure the assumption of harmonic vibration and to remove secular terms, the oscillating terms in (5) are omitted. The multinomial expansion are kept for $\{k_1, k_2, k_3\} = \{2, 1, 0\}$ and $\{1, 0, 2\}$, as this yields no oscillations. The next step is collecting (5) according to powers of ϵ in (6).

$$\begin{cases} \dfrac{\partial\varphi_0}{\partial T_0} = 0 \quad \Rightarrow \quad \varphi_0(T_1) \\ \dfrac{\partial\varphi_0}{\partial T_1} + \dfrac{\partial\varphi_1}{\partial T_0} + \dfrac{\lambda\varphi_0}{2} + \dfrac{\omega_i^2\varphi_{na0}}{2i\omega_i} - \dfrac{\omega_i^2\varphi_0}{2i\omega_i} = 0 \\ \dfrac{\partial\varphi_{na0}}{\partial T_0} + \dfrac{\lambda_{na}\varphi_{na0}}{2} + \dfrac{\omega_i^2\varphi_0}{2i\omega_i} - \dfrac{\omega_i^2(1+\kappa)\varphi_{na0}}{2i\omega_i} \\ \qquad + \dfrac{\omega_i^4\Omega}{i\omega_i^3}\left(\dfrac{3}{8}|\varphi_{na0}|^2\varphi_{na0} + \dfrac{3}{2}\varphi_{na0}\dfrac{\kappa}{\Omega}\right) = 0 \end{cases} \tag{6}$$

$$\begin{cases} \dfrac{\partial\varphi_0}{\omega_i\partial T_1} = -\dfrac{\xi\varphi_0}{2} + \dfrac{i\Phi_{na0}}{2} - \dfrac{i\varphi_0}{2} \\ 0 = -\dfrac{i(1-2\kappa) + \xi_{na}}{2}\Phi_{na0} + \dfrac{i\varphi_0}{2} + \\ \quad \dfrac{3i\Omega}{8}(|\Phi_{na0}|^2\Phi_{na0}) \end{cases} \tag{7}$$

In the first equation of (6) it is seen that φ_0, the major contribution to φ, only varies over the slow

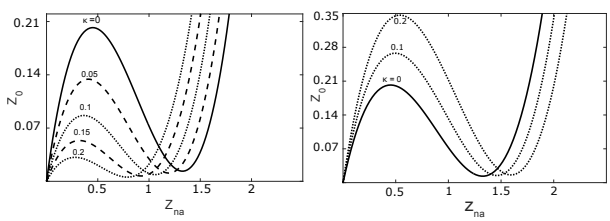

(a) (b)

Figure 1: The SIM for vibrations around $x^{*,2,3}$ (a), the SIM for vibrations around $x^{*,1}$ (b)

time scale T_1. The other two equation feature both the derivatives in T_0 and T_1 and are coupled in φ_0, φ_1 and φ_{na0}. It is proven in [3] that both φ_{na0} and φ_1 evolve towards a steady state as $T_0 \to \infty$; $\lim_{T_0\to\infty} \varphi_{na0} = \Phi_{na0}$ and $\lim_{T_0\to\infty} \varphi_1 = \Phi_1$; so that the dynamics of (6) can be written in steady state form of T_0, solely changing on the slow time scale T_1, yielding (7), with $\xi = \frac{\lambda}{\omega_i}$ and $\xi_{na} = \frac{\lambda_{na}}{\omega_i}$. The complex variables are written in polar notation; $\varphi_0(T_1) = R_0(T_1)e^{i\delta_0(T_1)}$ and $\Phi_{na0}(T_1) = R_{na}(T_1)e^{i\delta_{na}(T_1)}$, R_0, R_{na}, δ_0, $\delta_{na} \in \mathbb{R}$. Then splitting (7) in real and imaginary parts yields after some calculations (8). By introducing the energy-like variables $E_0 = R_0^2$ and $E_{na} = R_{na}^2$and their dimensionless energy-like variables $Z_0 = \Omega R_0^2 = \Omega|\varphi_0|^2$ and $Z_{na} = \Omega R_{na}^2 = \Omega|\Phi_{na0}|^2$ (9) is obtained which describes the dynamics of the slow flow, the first stating that Z_0 always decreases, and the second a showing a static relation, a slow invariant manifold (SIM) relating Z_{na} and Z_0. For several κ, the SIM is plotted on Figure 1a.

$$\begin{cases} \dfrac{\partial R_0^2}{\partial T_1} = -\xi R_0^2 - \xi_{na} R_{na}^2 \\ R_0^2 = -\left[\xi_{na}^2 + \left(1 - 2\kappa - \dfrac{3\Omega}{4} R_{na}^2\right)^2\right] R_{na}^2 \end{cases} \tag{8}$$

$$\boxed{\begin{aligned} \frac{\partial Z_0}{\partial T_1} &= -\lambda Z_0 - \lambda_{na} Z_{na} \\ Z_0 &= \left[\xi_{na}^2 + \left(1 - 2\kappa - \frac{3}{4} Z_{na}\right)^2\right] Z_{na} \end{aligned}} \tag{9}$$

The SIM has two extrema as long as $\xi_{na} < \frac{1-2\kappa}{\sqrt{3}}$:

$$\begin{cases} Z_{na}^{\pm} = \dfrac{8(1-2\kappa)}{9} \pm \dfrac{4}{9}\sqrt{(1-2\kappa)^2 - 3\xi_{na}^2} \\ Z_0^{\pm} = \left[\xi_{na}^2 + \left(1 - 2\kappa - \dfrac{3}{4} Z_{na}^{\mp}\right)^2\right] Z_{na}^{\mp} \end{cases} \tag{10}$$

The performance of the system vibrating around x^{*1} will also be considered as a comparison. Also, in the multi-modal case, there will be resonance cascading, and only for the first mode in the cascade, the initial resting position is $x^{*,2,3}$. For the modes lower than the first cascades mode, the vibrations are around $x^{*,1}$, and therefor the SIM around this point for these modes should be considered, derived by defining $u = x_l + \epsilon x_{na}$ and $v = x_l - x_{na}$ at the start of this session:

$$Z_0 = \left[\xi_{na}^2 + \left(1 + \kappa - \frac{3}{4} Z_{na}\right)^2\right] Z_{na} \tag{11}$$

Examples of the SIM in (11) is found on Figure 1b. Notice the now the Z_0^+ increases in function of κ instead of decreasing as on Figure 1a.

4. Tuning and Performance measures

Both tuning and performance measures depend on the initial conditions. Although the tuning and performance is based on the formulas of the previous section, from the slow flow of the single mode vibrating systems, the tuning and performance is easily extended to multi-modal vibrating systems by considering the initial *modal* conditions $\dot{x}(0) = \sum_{k=1}^{n} \dot{x}^{[k]}(0) = \sum_{k=1}^{n} e_k \dot{q}_k(0)$, with $\dot{x}^{[k]}(0) = e_k \dot{q}_k(0) \in \mathbb{R}^n$ the hypothetical initial speed as if only mode k is present. The initial displacements can similarly be expressed as $x^{[k]}(0) = e_k q_k(0) \in \mathbb{R}^n$.

4.1 Tuning

To tune the NES for single-modal systems, the nonlinear coefficient has to be chosen such that $Z_0(0) \geq Z_0^+$, otherwise no TET occurs. [4]

$$k_{na} \geq \frac{m_{na}\omega_i^4 Z_0^+}{\dot{u}^2(0) + \omega_i^2 u^2(0)} \tag{12}$$

In the multi-modal case, the mode i which initiates the RCC has to be chosen. The initial conditions in (12) then corresponds to the modal initial conditions of mode i, $x^{[i]}(0)$ and $\dot{x}^{[i]}(0)$.

4.2 Performance

4.2.1 Energy dissipation

If TET is initiated, it will persist until the minimum of the SIM, visualised on Figure 1a and Figure 1b, is reached. Only a fraction of the energy has been dissipated during TET, being:

$$E_{TET} = 1 - \frac{Z_0^-}{Z_0(0)} = 1 - \frac{E_0^-}{E_0(0)} \tag{13}$$

4.2.2 Pumping and cascading time

From the slow flow dynamics and SIMs, (8) & (11), the following integral can found

$$I(Z_{na}) = \frac{27}{32}Z_{na}^2 - 3Z_{na}(1+\mathcal{K}) + \Big((1+\mathcal{K})^2 + \xi_{na}^2\Big)ln(Z_{na}) = C - \omega_i\xi_{na}T_1 \tag{14}$$

with $\mathcal{K} = \{-2\kappa, \kappa\}$ depending on the resting point, -2κ for $x^{*,2,3}$ and κ for $x^{*,1}$. From this relation, the time between two states of Z_{na} can be calculated. If TET is initiated, the SIM will be descended from $Z_{na}(0)$ until Z_{na}^+. The duration of TET, called pumping time, is then:

$$\epsilon T_{pump} = \frac{1}{2\pi\xi_{na}}\Big(I(Z_{na}(0)) - I(Z_{na}^+)\Big) \tag{15}$$

with T_{pump} relative to the period of the modal frequency, with $T_{pump}\frac{\omega_i}{2\pi}$ the time in seconds. By considering each modal initial condition separately, a pumping time can be calculated for each mode partaking in the cascade. The total time for resonance capture is simply the sum of all of these pumping times:

$$T_{cascade} = \sum_{k=1}^{i} T_{pump,k} \cdot \frac{\omega_k}{2\pi} \tag{16}$$

For the mode initiating the RCC, T_{pump} should be determined for its correct initial resting position, either $x^{*,1}$ or $x^{*,2,3}$. For all lower frequency modes, the T_{pump} is determined for vibrations around $x^{*,1}$.

5. Simulation and validation of Performance

The measures derived in the previous section are only valuable if they hold their merit in actual numerical simulations. Both the single mode and multi mode cases are simulated. It will be seen that both for single and multi-modal systems, a tuned bi-stable NES vibrating around its stable equilibrium mitigate vibrations a lot faster than either the monostable cubic power NES or the bi-stable NES in around the unstable equilibrium. Before numerical simulations, the performance is assessed in function of κ, negative linear part of the NES. On Figure 2d, the energy dissipation in function of κ

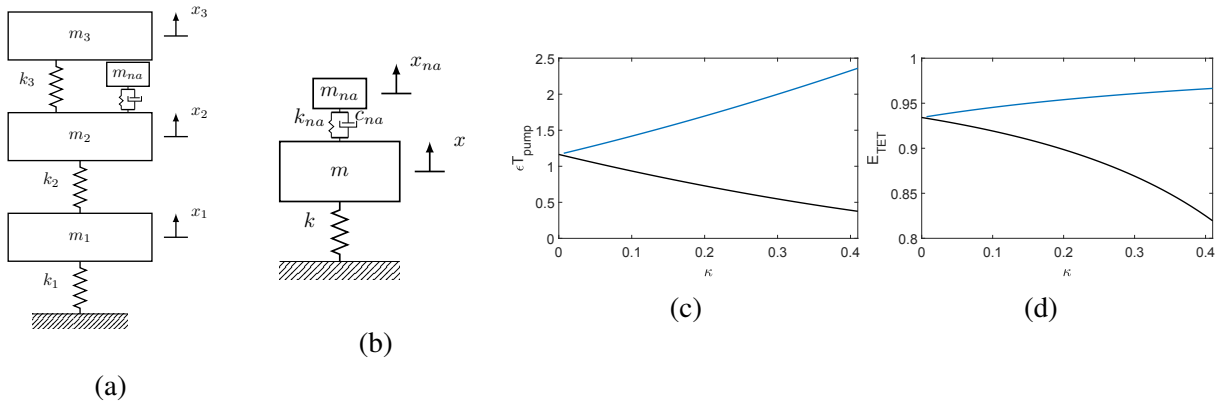

(a) (b) (c) (d)

Figure 2: The MDOF (a) and SDOF (b) system used in section 5 and the pumping time for $x^{*,1}$ (blue) and $x^{*,2,3}$ (black) (c) and the dissipated energy during TET for $x^{*,1}$ (blue) and $x^{*,2,3}$ (black) (d)

Table 1: Numerical values of single-mode system Figure 2b.

Coefficient	Value
$m\ [kg]$	1
$k\ [\frac{N}{m}]$	$4\pi^2$
$m_{na}\ [kg]$	0.02
$c_{na}\ [\frac{Ns}{m}]$	0.0065

κ	Z_0^+	k_3	k_{lin}	E_{TET}	T_{pmp}
0	0.2020	743	0	0.986	22.6
-0.1, $x^{*,1}$	0.1047	988	-0.079	0.988	27.38
-0.1, $x^{*,2,3}$	0.34670	381	-0.079	0.978	14.4

is shown for a perfectly tuned NES, $Z(0) = Z_0^+$. For vibration around $x^{*,1}$ the energy increases as κ increases, while the opposite holds for $x^{*,2,3}$. On Figure 2c, the pumping time in function of κ is shown for a perfectly tuned NES. For vibration around $x^{*,1}$ the pumping time increases as κ increases, while the opposite holds for $x^{*,2,3}$. While for vibrations $x^{*,1}$ more energy will be dissipated, it will be slower and while $x^{*,2,3}$ is faster, it will dissipate less energy. This will be validated in numerical simulation as well.

5.1 Single-mode vibrations

A NES is connected to a single mass-spring-damper, see Figure 2b, with parameters found on Table 1. The NES is tuned for such that $Z_0(0) = Z_0^+$ for an initial speed of $\dot{x}(0) = 0.1\ \frac{m}{s}$, with the coefficients, energy dissipation and pumping time also found on the same table. The system is numerically simulated with the main system's and NES's vibration shown on Figure 3a. The predicted pumping time is clearly seen in the main system's vibration as approximately the moment the vibration stop decreasing rapidly, indicating TET has ceded. For lower predicted energy dissipation, the residual vibration energy is clearly higher. To compare the slow flow dynamics (9) or (11) with the actual numeric simulations, simulations of the slow flow are overlayed with the *Hilbert* transform of the actual dynamics on Figure 3b. A good accordance is found, showing that the simplified slow flow dynamics are representative for the actual dynamics.

Table 2: Numerical values for MDOF and absorber system, Fig.2a.

Coefficient	Value
$m_k\ [kg]$	1
$k_k\ [\frac{N}{m}]$	1
$m_{na}\ [kg]$	0.06
$c_{na}\ [\frac{Ns}{m}]$	0.0108

κ	k_p	k_{lin}	$T_{pmp,3}$	$T_{pmp,2}$	$T_{pmp,1}$	T_{cas}
0	74.1	0	21.8	140	1066	1227
-0.1, $x^{*,1}$	98.2	-0.0195	26.5	158	806	991
-0.1, $x^{*,2,3}$	38.4	-0.0195	13.6	57.1	331	402

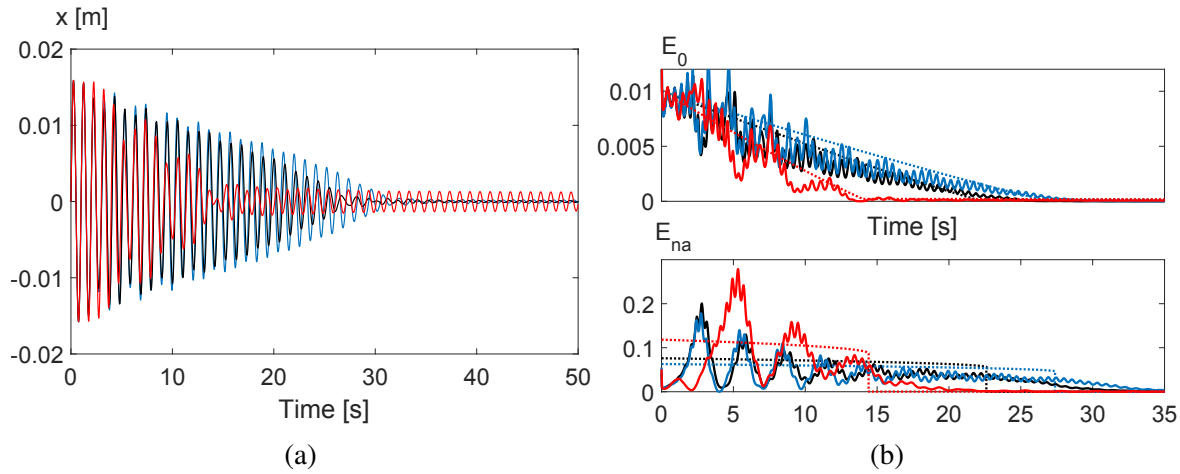

Figure 3: Main system vibration (a) for $\kappa = 0$ (black), $\kappa = -0.1$ and $x^{*,2,3}$ (red) and $\kappa = -0.1$ and $x^{*,1}$(blue). Comparison slow flow (dotted) and simulation (full) (b).

.

5.2 Multi-modal vibrations

On the 3DOF system on Figure 2a, a NES is connected to x_2. The NES is tuned in order to start cascading at mode 3. This way, all modes will engage in the cascade and will be dissipated. The coefficients, pumping time of each mode and cascading time are given in Table 2 for an initial speed of $\dot{x}_1 = 0.1\ \frac{m}{s}$, such that $\dot{x}_2^{[3]} = -0.046$ is used for tuning. The bi-stable NES is predicted to cascade faster (for both unstable and stable equilibria) then the cubic NES. Numerical simulations of the bi-stable NES initially in its stable resting point show that the cascading time is a good predictor for when the vibrations of the main system Figure. 4a stops decreasing significantly, with the cascading time highlighted with a line. The NES vibrations, Figure 4b, illustrate the resonance cascade, it starts vibrating with the 3rd mode first, then cascades to mode 2 and finally mode 1, and stops vibrating significantly after the cascading time. The cascade is better seen by looking at the wavelet transforms 4c and 4d, which reveals the change of frequency of the NES vibration over time. The wavelet transform show the jump in modal frequencies the NES vibrates with. Each mode vibrates approximately as long as the calculated pumping time for each mode. Although the cascading time is only approximately predicts the actual cascading time, it is a suitable measure of the cascading speed.

6. Conclusion

The performance of a bi-stable NES in mitigating vibrations of a mechanical system was investigated, for the bi-stable NES in both stable and unstable equilibrium. The derived measures allowed to asses the energy dissipated and the duration of TET for a single mode and the duration of RCC for multiple modes. By comparing these measures with numerical simulation, it was shown that these algebraic measure hold their merit. It was shown with the performance measures and validated with the simulations that a bi-stable NES initialized in its stable equilibrium, is faster then when initialized in its unstable equilibrium or a NES with cubic nonlinearity.

REFERENCES

1. Vakakis, A. F., Gendelman, O. V., Bergman, L. A., McFarland, D. M., Kerschen, G., and Lee, Y. S. Nonlinear targeted energy transfer in mechanical and structural systems. *Springer Science & Business Media*, (2008)

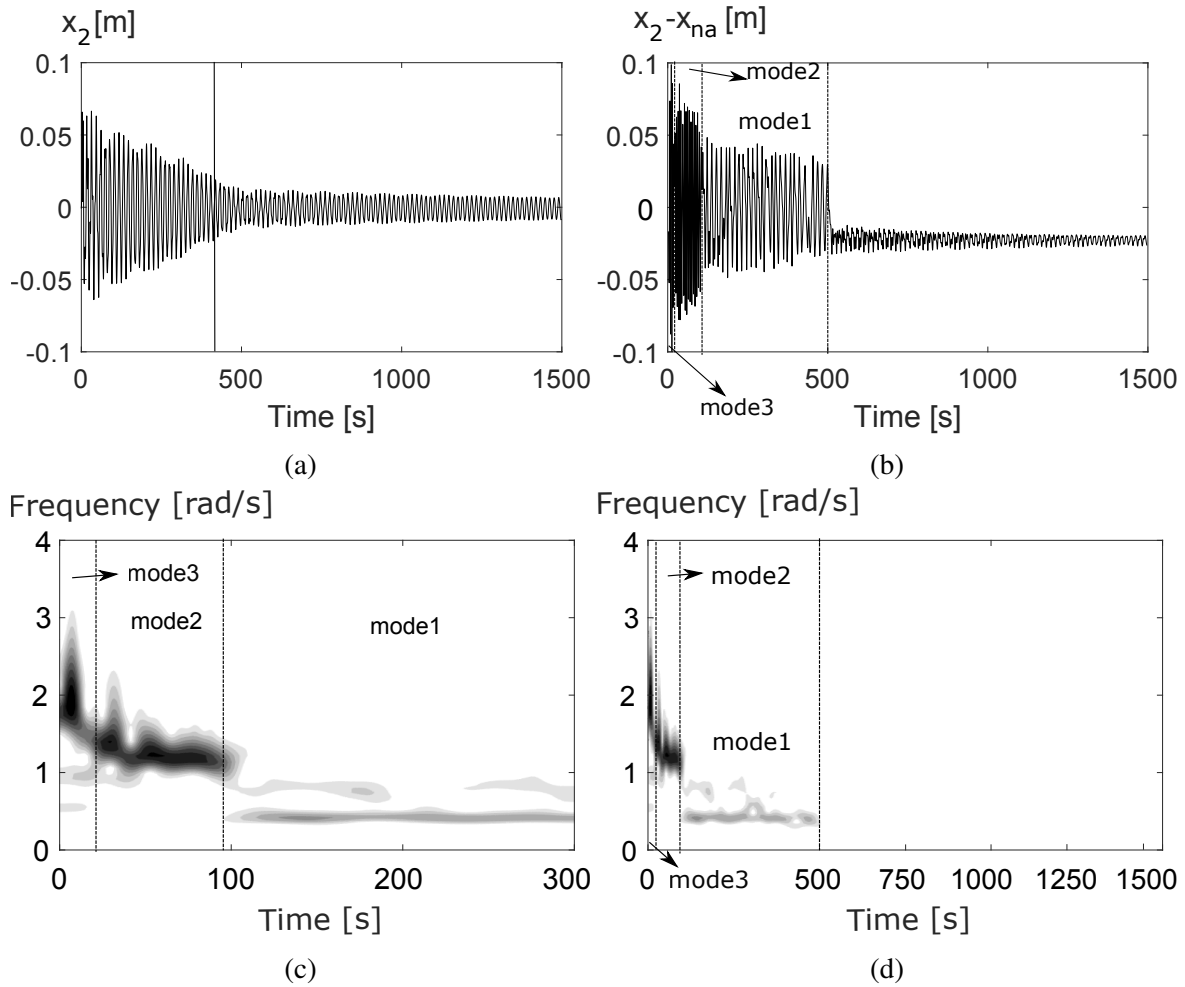

Figure 4: Result of numerical simulation on MDOF system Figure 2a, (a) are the displacements of x_2, (b) of the NES and (c)(d) wavelet transform of the NES

2. Manevitch, L. I., Sigalov, G., Romeo, F., Bergman, L. A., and Vakakis, A. Dynamics of a linear oscillator coupled to a bistable light attachment: analytical study, *Journal of Applied Mechanics*, **81** (4), 041011, (2014)

3. Gendelman, O.V. Bifurcations of nonlinear normal modes of linear oscillators with strongly nonlinear damped attachment, *Nonlinear dynamics*, **37** (2), 115–128, (2004).

4. Nguyen, T. A. and Pernot, S. Design criteria for optimally tuned nonlinear energy sinks?part 1: transient regime, *Nonlinear Dynamics*, **69** (1), 1–19, (2012)